A Wall Effects and Means of Controlling the Evolution of Swirling Flows with Vortex Breakdown

A. Meziane[1], M. Hachemi[2†], M. Kessal[3] and M. Imoula[1]

[1]*Dynamique des Moteurs et Vibroacoustique Laboratory, M'Hamed Bougara Boumerdes University, Algeria*
[2]*Energétique, Mécanique et Ingénieries Laboratory, M'Hamed Bougara Boumerdes University, Algeria*
[3]*GéniePhysique des Hydrocarbures Laboratory, M'Hamed Bougara Boumerdes University, Algeria*

†Corresponding Author E-mail: ma.hachemi@univ-boumerdes.dz

ABSTRACT

This paper investigates numerically the bubble-type vortex breakdown apparition in the case of closed rotating flows of a viscous, axisymmetric, and incompressible fluid. First, a truncated conical/cylindrical cavity of spherical end disks is used to simulate and analyze the vortex structure under rigid surface conditions. The geometric effects of the enclosure are also studied. Vortex breakdown is demonstrated beyond the lower disk rotation rate threshold by introducing the no-slip condition imposed on the upper wall. The objective is to explore ways of controlling the evolution of this physical event by modifying the confinement conditions upstream of the vortex rupture. Particular attention is also paid to the effective kinematic viscosity, thermal diffusivity and geometric control of recirculation zones on the axis of rotation (axial bubble type). The second geometry consists of a spherical annulus formed by two concentric hemispheres in differential rotation under plat-free surface conditions. The results show that rotation of the inner hemisphere induces a vortex bubble on the polar axis. In contrast, the outer hemisphere rotation induces a toroidal vortex on the equator.

1. INTRODUCTION

The confined swirling flows with vortex breakdown covers many engineering applications, such as biochemical combinations, substance transformations, pharmacology and mixture preparation. In the vicinity of the critical Reynolds number, the size of the central viscous core increases with the angular velocity imparted to it and gives rise to a type of bubble located on the polar axis of rotation, characterised by stagnation points, frequently referred to as vortex decomposition (Leibovich, 1978). Vortex breakdown has been considered as a key to understanding the fundamental mechanisms involved in the process of transition from flow to turbulence. A particular approach has been devoted to this physical event, characterised by a sudden change in fluid behaviour. It was first observed by Vogel (1968) in a flow pattern realised by the counter rotation of a single disc in a cylindrical enclosure. Vogel's flow visualisation tests clearly demonstrated the appearance of an individual recirculation zone. A perfect picture based on the visualisation of the flow field was determined by Escudier (1984). He noted different regimes where the flow is axisymmetric in the steady state and at notable penetrations into the unsteady domain. Most of the subsequent research (Escudier, 1984; Lopez, 1990) has been based on the Vogel experiment. It shows precisely the conditions of confinement and allows the comparison of numerical and experimental simulations. In this model, the occurrence of vortex ruptures (one, two or three) depends on the cavity aspect ratio and the Reynolds number. Several studies have applied it to the study of flows in close geometries.

Previous numerical or experimental investigations (Yalagach & Salih 2016) confirmed that vortex breakdown occurs for certain combinations of these two parameters (Ah, Re). Different areas of one or more vortex structures are mapped on the rotation axis. A three-dimensional flow pattern and the structure of the associated recirculation regions in a cylindrical enclosure with a large axial aspect ratio were studied numerically by Serre & Bontoux (2001). Bhaumik & Lakshmisha (2007) extended the work of Escudier (1984) using the lattice Boltzmann method (LBE). The authors reported a much wider range of parameters to trace the existence of one or more vortex bubbles and stable and unstable flow regions. While several numerical or experimental works

have been devoted to cylindrical cavities, other geometric shapes have not been well explored. Relatively little work is done that takes into account the problem of cavity asymmetry or symmetry. Bühler (2009) presented an experimental model of a rotating flow in a conical cavity with a rotating spherical wall.

Different paths of inspecting vortex breakdown in confined flows have been proposed, employing various techniques. Escudier et al. (2007) numerically investigated the effects of converging and diverging geometry on secondary flow with wall rotation. Several experimental and numerical studies have proposed other geometric configurations, including a rotating conical bottom (Pereira & Sousa 1997; Rudolf, 2008; Sousa, 2008) to stabilise the occurrence and evolution of recirculation zones.

Other non-intrusive methods of controlling vortex breakdown are founded on the effect of a small fixed rod placed in axis of the cylinder (Cabeza et al., 2005; Sturzenegger et al., 2012) or via the addition near the axis of a co-or-counter-rotation rod of different sizes with rotating bottom endwall (Husain et al., 2003; Jacono et al., 2008; Dash & Singh 2018) or based on the differential rotation of a small disk of different sizes migrated in the non-rotating upper disk (Mununga et al., 2014). These methods show a suppressive or stimulating effect on vortex breakdown. Meunier & Hourigan (2013) studied experimentally and theoretically the effect of combining properties of the fluid in a cylindrical cavity with a tilt angle of the rotating or stationary disk. Their results indicate that the flow homogenization time is strongly influenced by the degree of inclination of the rotating end disks and by the absence and/or presence of a vortex breakdown. The stability and comportment of a reverse area were studied by Dash & Singh (2018) in a cylindrical annulus in the case of a thin axial rotating or stationary rod.

In a cylindrical geometry, the application of an axial temperature gradient while the sidewall is thermally insulated (Herrada & Shtern 2003) reveals that a small positive vertical temperature gradient suppresses bubbles. In contrast, a negative gradient tends to favour their

appearance. Turan et al. (2018) numerically investigated the effects of wall heating in several classes of cylindrical vessels, where flows are driven by the rotation of one of the end discs. The latter are fixed at different thermal and kinematic boundary conditions. Their results indicate that the rate of heat transfer has a spectacular effect when the cavity lid is rotated and kept hot or cold. Dash & Singh (2016) studied the development of the recirculation bubble in the Boussinesq flow under axial heat flow when the sidewall is perfectly insulated. Their study was carried out in the case of rotation and heating of the upper disc. Yu et al (2013) analysed the influence of a uniform magnetic field in the axial direction on the vortex structure generated by the rotating upper disc of a confined cylindrical cavity. The authors concluded that the increase of the Hartmann number, leads to the disappearance of the vortex breakdown.

The objectives of this work are twofold. First, we aim to validate our numerical simulation results with the experimental work of Bühler (2009). Secondly, we study the rupture of vortices on the axis for cavities with curved walls and filled with a viscous fluid.

Depending on the nature of this work, a set of dimensionless parameters which are named as follows: Reynolds number, rotation rate ratio of an upper disk, of the conical disk and the sidewall, two hemispheres concentric, radius ratio, angle of the sector, and characteristic lengths of the cavity. They characterize the movement of the fluid and they are defined respectively by $Re=\Omega_b R_{0b}^2/v$, $S=\Omega_t/\Omega_b$, $SC=\Omega_c/\Omega_b$, $SL=\Omega_L/\Omega_b$, $So=\Omega_t/\Omega_b$, $\alpha=R2/R1$, $\theta0$, $R0t=R1\sin\theta0$, $R0b=R2\sin\theta0$. They can be combined to give another common non-dimensional group with the Rayleigh number Ra and Prandtl number Pr. We note $Ra= g\ \beta(Tb-Tt)\ R_{0b}^3/v\lambda$, $Pr=v/\lambda$, where g, β and λ are named respectively: the acceleration due to gravity, the thermal expansion coefficient, and the thermal diffusivity. The effect of sidewall inclination is examined by varying the angle of the spherical sector. This leads to the variation of the characteristic length parameters in the truncated cone cavity. In addition, the sensitivity of on-axis bubbles in
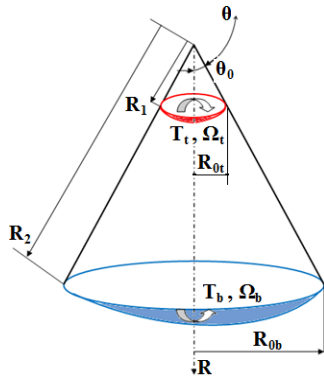
Fig. 1(a) Base schematic of the problem with parameters in case of heating
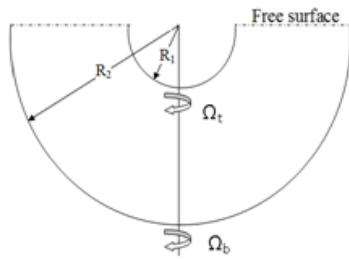
Fig. 1(b) Schematic of hemispheres with free surface

the spherical sector geometry with a low-temperature gradient is investigated.

2. MATHEMATICAL FORMULATIONS

We consider the flow in a cone-shaped enclosure, enclosed by spherical lids, with radii R1 and R2= 300 mm. They rotate at different rotational speeds Ωbottom and Ωtop (Fig. 1a). The thermophysical properties are assumed to be constant and the flow is assumed to be quasi-stationary in the laminar range. Numerical results obtained in confined cavities are presented in several geometrical configurations. We note that R0t= R1sinθ0, R0b= R2sinθ0 corresponds to the tronconical enclosure; R0t= R0b= R1sin θ0 corresponds to the cylindrical cavity, and the hemispherical ring geometry is considered when θ0 =90° (Fig. 1b).

The velocity components in the three directions (r, θ and Φ) are (u, v and w) respectively. For an incompressible flow, in a two-dimensional plane (r,θ) the three components of the velocity in agreement with the continuity equation, being coupled with the current function $\Psi(r,\theta)$ and the vortex function $\Omega(r,\theta)$, as follows:

$$u(r,\theta)=\frac{1}{r^2\sin\theta}\frac{\partial\psi}{\partial\theta} \ , \ v(r,\theta)=-\frac{1}{r\sin\theta}\frac{\partial\psi}{\partial r} \ , \ w(r,\theta)=\frac{\Omega}{r\sin\theta}$$

as the flow is considered to be unattached of the (1)
longitudinal direction Φ, the governing equation of the flow can be written as:

$$\frac{\partial\Omega}{\partial t}r^2\sin\theta+\frac{\partial(\psi,\Omega)}{\partial(r,\theta)}=\frac{r^2\sin\theta}{Re}D^2\Omega \quad (2)$$

$$\frac{\partial\zeta}{\partial t}\cdot r^2\sin\theta+2\Omega\left(\cot\theta\frac{\partial\Omega}{\partial r}-\frac{1}{r}\frac{\partial\Omega}{\partial\theta}\right)+2\zeta\left(\cot\theta\frac{\partial\psi}{\partial r}-\frac{1}{r}\frac{\partial\psi}{\partial\theta}\right)-\frac{\partial(\psi,\zeta)}{\partial(r,\theta)}$$

$$=\frac{r^2\sin\theta}{Re}D^2\zeta \quad (3)$$

$$\frac{\partial T}{\partial t}+u\frac{\partial T}{\partial r}+\frac{v}{r}\frac{\partial T}{\partial\theta}=\frac{1}{RePr}\left(\frac{\partial^2 T}{\partial r^2}+\frac{2}{r}\frac{\partial T}{\partial r}+\frac{1}{r^2}\frac{\partial^2 T}{\partial\theta^2}+\frac{1}{r^2}\cot\theta\frac{\partial T}{\partial\theta}\right) \quad (4)$$

$$\zeta=D^2\psi \quad (5)$$

where D^2 is the operator:

$$D^2=\frac{\partial^2}{\partial r^2}+\frac{1}{r^2}\frac{\partial^2}{\partial\theta^2}-\frac{\cot\theta}{r}\frac{\partial^2}{\partial\theta^2} \ et \ \frac{\partial(\psi,\Omega)}{\partial(r,\theta)}=\frac{\partial\psi}{\partial r}\frac{\partial\Omega}{\partial\theta}-\frac{\partial\psi}{\partial\theta}\frac{\partial\Omega}{\partial r}$$
(6)

The non-dimensional border and starting conditions for the above governing assimilations are:

at the axis θ_0 =0:

$$\psi=0, D^2\psi=0, \Omega=0 \quad (7\text{-a})$$

at the top disk for different cavities R=R$_1$, $\forall$ θ_0:

$$\Omega(R_1,\theta)=\Omega_t\sin^2\theta, \psi(R_1,\theta)=\frac{\partial\psi}{\partial R}(R_1,\theta)=0 \quad (7\text{-b})$$

at the bottom disk for different cavities R=R$_2$,$\forall$ θ_0:

$$\Omega(R_2,\theta)=\Omega_b\sin^2\theta, \psi(R_2,\theta)=\frac{\partial\psi}{\partial R}(R_2,\theta)=0 \quad (7\text{-c})$$

at the sidewall of conical cavity θ_0 =15°, R$_1\leq$R$\leq$ R$_2$:

$$\Omega(R,\theta_0)=\Omega_L R^2\sin^2\theta_0,$$
$$\psi(R,\theta_0)=0, \frac{\partial\Psi}{\partial\theta}(R,\theta_0)=0 \quad (7\text{-d})$$

at the sidewall of cylindrical cavity θ_0 =20°, R$_{0t}$= R$_1$sin θ_0:

$$\Omega(R_{0t},\theta_0)=\Omega_L R_{0t}^2,$$
$$\psi(R_{0t},\theta_0)=0, \frac{\partial\Psi}{\partial\theta}(R_{0t},\theta_0)=0 \quad (7\text{-e})$$

at free surface of the hemispheres θ_0=90°,

R$_1\leq$R$\leq$ R$_2$: $\Psi(R,\theta_0)=0, \frac{\partial\Omega}{\partial\theta}=0$ (7-f)

Thermal Boundary Conditions

at the axis θ_0 =0°, R$_1\leq$R$\leq$ R$_2$: $\frac{\partial T}{\partial\theta}=0$ (7-g)

at side wall θ_0 =15°, R$_1\leq$R$\leq$ R$_2$: $\frac{\partial T}{\partial\theta}=0$ (7-h)

at the top and bottom disk:

$$Ra \succ 0 \begin{cases} R=R_1, 0\leq\theta\leq15°, T=1 \\ R=R_2, 0\leq\theta\leq15°, T=0 \end{cases}$$
(7-i)

$$Ra \prec 0 \begin{cases} R=R_1, 0\leq\theta\leq15°, T=0 \\ R=R_2, 0\leq\theta\leq15°, T=1 \end{cases}$$
(7-j)

(a)   (b)
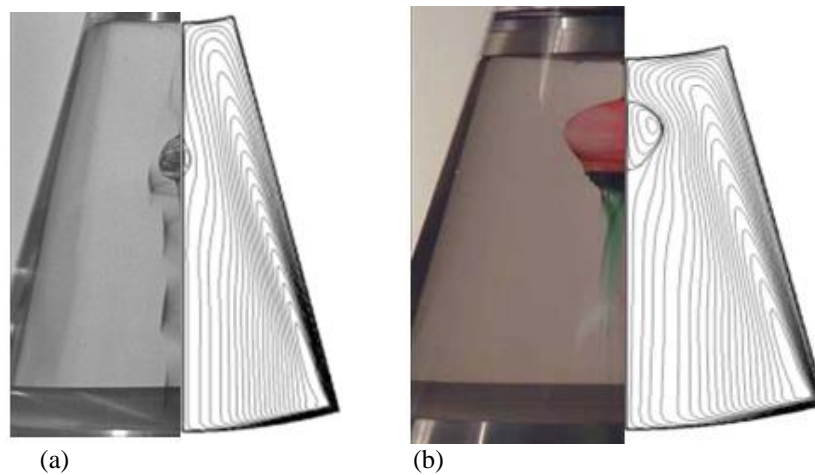
Fig. 2 Meridian streamlines for θ_0= 15 (a) α= 3.06, Re= 5000; (b) α= 2, Re = 3600. In qualitative agreement with experimental flow visualisation taken from Bühler (2009)

Table 1 Mesh characteristics for the case α=2, Re = 644

(r×θ)	A(60×30)	B(80×40)	C(100×60)	D(150×110)	E(200×150)
$\Psi_{max}(10^{-5})$Kg/S	1.66768	1.653139	1.643687	1.608053	1.59475
Nodes used	1891	3200	6161	16761	30351

3. RESULTS AND DISCUSSIONS

3.1 Numerical Method and Validation

The equations governing the flow are discretised by the finite difference method, the numerical algorithm of this method consists of three steps (Imoula et al., 2016), to solve the partial nonlinear mathematical problem. Structured grids are used. It should be noted that the solution time obviously depends on the number of cells. The structured mesh consists of (120×60) elements for the truncated conical container. Numerical calculation tests were taken with A (60×30), B (80×40), D (150×110), and E (200×150) uniform cells to research the precision of our calculations in a cylindrical cavity. A series of quantitative estimations of a maximal contour of Ψ (Table 1) shows that the error between D (150×110) and E (200×150) is about 0.8% at more and that may be considered as negligibly weak. E (200×150) mesh grid is used for the results reported in our solution.

The visualisation shows the spiral character of the flow directed from the top to the bottom of the cavity (Bühler, 2009). The constitution of the vortex structure changes depending on the confining conditions and the physico-geometric parameters. Figure 2 shows a comparison with the experimental visualisations of Bühler (2009); the right and left meridians of the flow (symmetrical to the centre of the enclosure) are shown. They are obtained by modelling the confined flow specified by: θ0= 15 (a) α= 3.06, Re =5000; (b) α=2, Re= 3600. The structure of the studied flow is in qualitative agreement with the axisymmetric flow pattern mentioned by Bühler (2009). The conical geometry allows to study this phenomenon also in a region between two concentric hemispheres with a free surface.

3.1.1 Influence of Rotation of the Top

A recirculation bubble is shown on the axis of rotation. This region is closer to the fixed lower disc at about R= 0.265 (Fig. 3a). The recirculation regions (Fig. 3b) indicate that the co-rotation of the spherical bottom cover is sufficient to improve the dimensions of the recirculation zones. Thus, a bubble with an enlarged vortex structure is formed for Sb≤0.1. A corner vortex emerges in the lower right corner of the transverse division. For larger differential rotations (Sb>0.1), the outward flow over the lower disc causes a downward radial flow near the axis of symmetry of the truncated enclosure. The qualitative structure of the flow contains two dominant, co-rotating cells resulting from the competition of centrifugal circulations induced by the two spherical discs and a single reduced zone attached to the axis of rotation, deduced from the influence of co-rotation (Fig. 3c, d). The cells are separated by a stagnation line ψ=0, connecting the stagnation points.

3.1.2 Influence of Rotating Conical Endwall

The truncated conical cavity validated above is changed by inserting an upper cone-shaped lid of elevation h_c in lieu of spherical disc. The cone can revolve with a spinning report of S_c within the field -0.2≤ Sc ≤0.2. The sidewall is stationary. The conical top lid has a dominant influence on vortex breakdown formation (see Fig. 4). With the identical parameters of Re and R_{0b}, calculations exhibit that, considering it increases, the motionless cone-shaped lid (Sc=0) causes a displacement down of the recirculation zone. Then, it diminished in size (Fig. 4c) and eventually suppressed at h_c =0.04. The latter is not displaced, since the distance of its trailing edge stagnation point to the rotating disk remains constant.

Regarding the impact of changing the kinematic status upstream of the recirculating region, the meridianal stream contours reveal that co-rotation enhances the vortex structure, giving rise to another enlarged vortex breakdown bubbles (Fig. 5b, c).

(a) $S_b=0$ (b)$S_b=0.1$ (c)$S_b=0.2$ (d)$S_b=0.3$
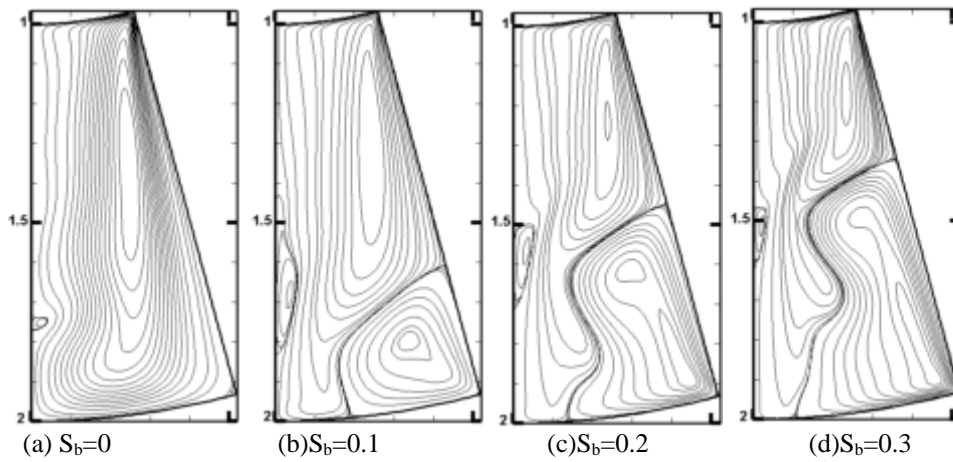
Fig. 3 Stream contours presents the effect of differential rotation of rotating bottom disk for α=2, θ₀=15°, Re=3600. The rotation rate ratio S_b is indicated

(a)$h_c=0$ (b)$h_c=0.01$ (c)$h_c=0.02$ (d)$h_c=0.04$
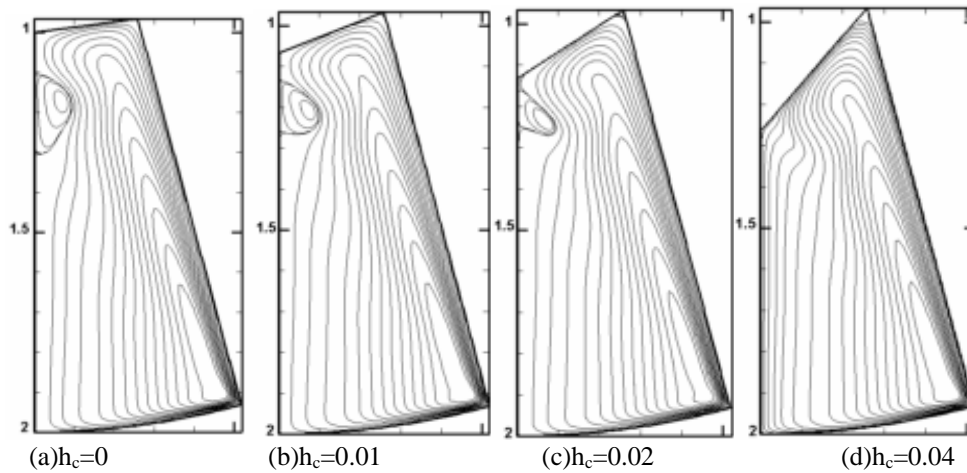
Fig. 4 Stream contours presents the effect of top conical lid for α=2, θ₀=15, Re=3600. The height of the cone h_c is indicated

By contrast, the Fig. 5d shows that a relatively feeble counter-motion of the upper cone-shaped lid is adequate to eliminate the vortex breakdown while sustaining stable flux. A radial displacement is viewed in the process. The vortex structure is removed when the cone counter- spinning arrives roughly 1.3% of the background disc. The differential rotation leads a significant modification on the flow, in particular, the meridian movement generated by the co-counter-rotating of the two end discs provokes to accelerate the transport of the angular movement and the axial flow, which prevents the fluid from stagnating on the axis and consequently eliminates or promotes the reverse splitting zones. In addition, co-rotation stimulated to push the breakdown bubble upwards away from the rotating end wall, while counter rotation causes the bubble to migrate downwards.

(a) $S_c=0$ (b) $S_c=0. 13$ (c) $S_c=0.2$ (d) $S_c=-0.13$
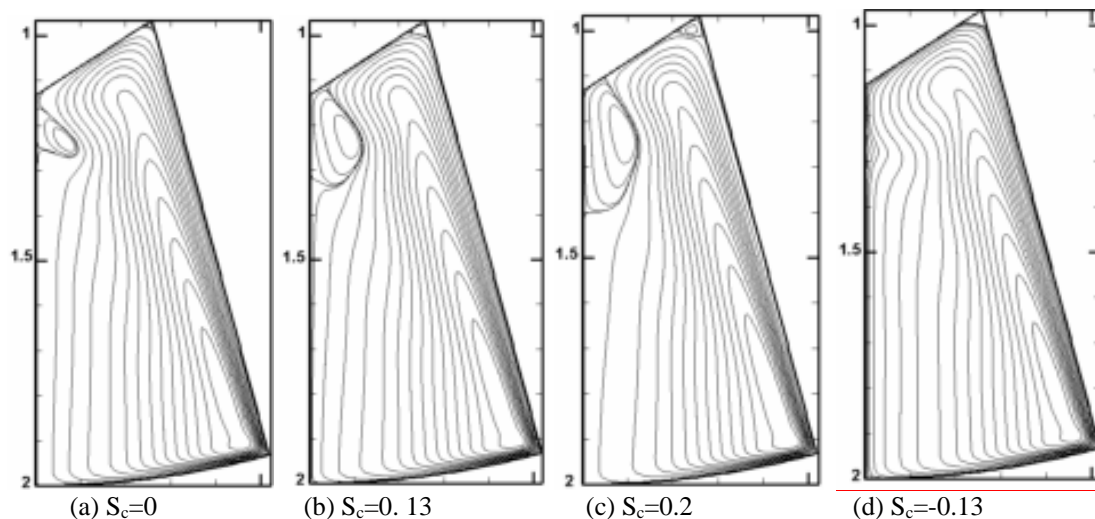
Fig. 5 Stream contours presents the effect of differential rotation of top conical disk for Re=3600, α=2, θ₀=15°at h_c=0.02. The rotation rate ratio S_c is indicated
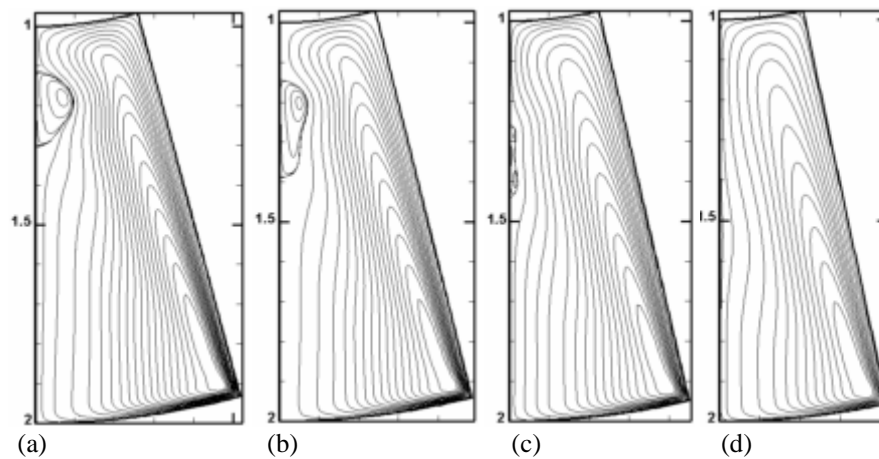
Fig. 6 Streamlines for narrowing geometry for Re= 3600, α=2, (a) θ_0= 15, R_{0b}= 77.65 mm, (b) θ_0= 14, R_{0b}= 72.56 mm, (c) θ_0=13, R_{0b} =67.48 mm, (d) θ_0= 12, R_{0b}= 62.37 mm

3.1.3 Influence of the Narrowing Sidewall

A spherical lid-driven swirling flow 2 in the above-described truncated cone cavity radius ratio at Reynolds number Re = 3600 is considered to investigate the effect of narrowing stationary sidewall. For a specified ensemble of parameters, it shows a single bubble on the rotating axis of the cavity. To modify the radial eddy upstream of the vortex structure, the characteristic lengths parameter of lower disk R_{0b} of the resulting narrowing truncated conical enclosure is changed in the gamut 62.37 mm $\leq R_{0b} \leq$77.65mm (who equivalent to an incline geometrical relation 12°$\leq \theta_0 \leq$15°) (Fig. 6). The case with θ_0=15°, R_{0b}=77.65 mm corresponds to the situation where there is no slope on the immobile side wall of the truncated conical pattern (Fig. 6a). It clarifies the lines of current correspond to the exemplary of flux conducted per the spherical background end disk. It is remarked that a relatively feeble disturbance causes great and pertinent alterations to the vortex breakdown phenomena. As a matter of fact, for R_{0b}= 72.56 mm, θ_0=14° and R_{0b}= 67.48 mm, θ_0= 13°, Fig. 6b and Fig. 6c indicate a substantial dimension depletion of the vortex structures, accompanied by a displacement radially down. The significant value R_{0b}= 62.37 mm (θ_0= 12°) (Fig.6d) provokes the cancellation of vortex breakdown bubble.

Quantitatively, the axial speed profile component, on the axis of the cavity (Fig. 7) clearly explains the vanishing of stagnation points on the axis, characterizing confined vortex bursts. It can be remarked that the axial velocity profiles confused in the vicinity of the spherical end discs (0.15 $\leq R \leq$ 0.16, 0.29 $\leq R \leq$ 0.3) indicated a similar axial acceleration of fluid in these regions. At exterior of these axial regions, $|w|$ increases under the control of narrowing of the sidewall and the flow is down, without inverse regions. As a result, we note that that the inclination effect helped to intensify the axial flow descending from the fixed disc.

3.1.4 Control of Vortex Breakdown by Thermal Convection

This numerical step consists the controlling the vortex breakdown behaviour under the influence of parietal thermal forcing using a radial temperature gradient on the truncated
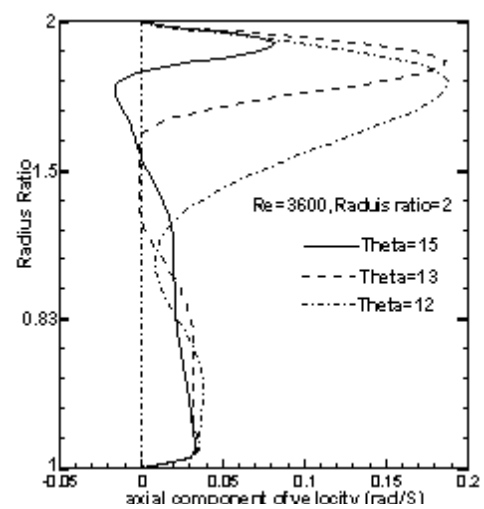
Fig. 7 Axial velocity profiles at θ_0= 0, forRe= 3600, α= 2

conical enclosure together with a rotation of the bottom lid. The confined swirling flow motifs in addition to the heat transfer effect are numerically examined below the Boussinesq hypothesis. The underlying mechanism of such recirculating region supervision is based on centrifugal and gravitational convection. Steady-state axisymmetric solutions are obtained at the identical parameter values like in the (Fig. 2a): Reynolds number 5000, Prandtl number 1.0 and for a cavity of radius ratio 3.06. We note that (Ra< 0) is referred to when the surface of the bottom rotating disk is preserved in at lower temperature as compared to the top unmoving disk, while (Ra>0) is referred to a warmer bottom rotating lid than the spherical top. With the addition of a temperate positive and/or negative radial temperature gradient, a coupling between heat flow and the flow velocity begins affecting each other, which can significantly diminish (enforce) the vortex breakdown bubble. Let us talk in the next paragraph on process of vortex breakdown development and cancellation. Let us talk in the next paragraph on process of vortex breakdown development and cancellation. For a positive vertical temperature gradient *(Ra > 0)*, the sense of the control flow (analogous to that in Fig. 2a) is converse to that of the basis flow outside the recirculation bubble region (Fig. 8b, c).

The effect of such a check flow decreases the force of meridional movement. As results, both the radial and tangential swirls transport from the revolving lower disc to the top gets poor. An extra essential characteristic of check flows is their
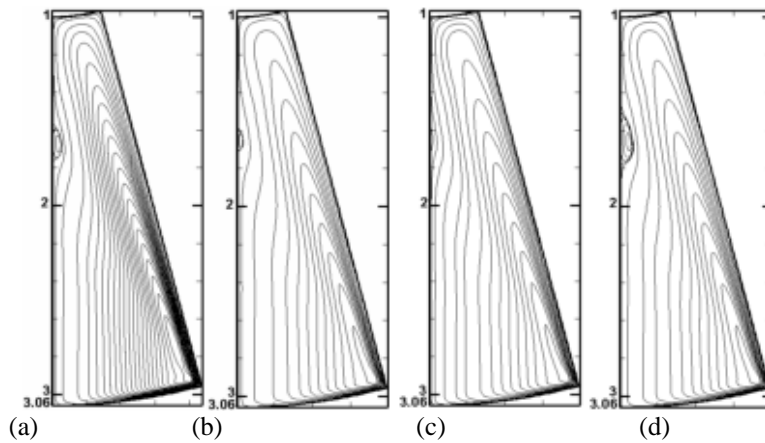
Fig. 8 Contours of steam function for different Ra: a) Ra = 0, b) Ra =7.12×10 ^{3}, c) Ra = 1×10^4, d) Ra = -1.2×10^4, for Re =5000, θ_0=15, α=3.06.

mass convergence towards the rotation axis. It decreases the distribution of the lines of current away from the center, which is characteristic of a main flow. For a negative (Ra< 0) radial temperature gradient, the supervision flow has the same sense as the main meridional current. It strengthens the angular momentum transportation from the base disk toward the top disk and afterwards to the centre. It causes a greater accumulation of vorticity in the vortex nucleus. Such concentration ensues from the enhancement of vortex breakdown (Fig. 8 d).

Stages of bubble suppression as the Rayleigh number increases are shown in Fig. 9. The motion of the fluid in the wide part, apart from the discs, tends to slow down considerably as indicated by the distribution of the speeds in Figs. 9. This comportment is contrary to the isothermal case (Ra = 0), where the wide part of the fluid undergoes a motion of angular velocity intermediate to that of the discs. Examining the change in the axial component of the velocity alongside of truncated conical center for the curve Ra = 1×10^4 (Fig. 9) and the vortex structure presentation (Fig. 8c), it can be seen that the pumping of Ekman be disposed to vanish due to the blocking of the axial movement due to the impacts of buoyancy.

3.2 Basic Flow in a Cylindrical Cavity

3.2.1 Description of a Cylinder Flow Driven by a Spherical Bottom Disk (S$_b$=0)

The stable exemplary flow entrained by a cylindrical enclosure's spherical bottom is exhibited for a range of particular parameters 1.48≤ α ≤3.06, 418≤Re≤767. It should be noted that these geometries correspond to these parameters are an extension of the conical sector validated above.

In addition to an azimuthal movement, which the fluid gains initially at the rotating bottom disk, it evolves a secondary movement together with a concentrated centric vortex kernel. The latter ruptures to donate birth to single, double, and triple distinct on-axis bubbles as defined by Escudier (1984) and reminiscent of a B-type vortex breakdown defined by Leibovich (1978) (Fig. 10 and Fig. 12).

When meridian steam contours are plotted, they are non-uniformly discarded to underline the relatively feeble but appropriate backflow regions. The evolution of the vortex breakdown can be associated with a
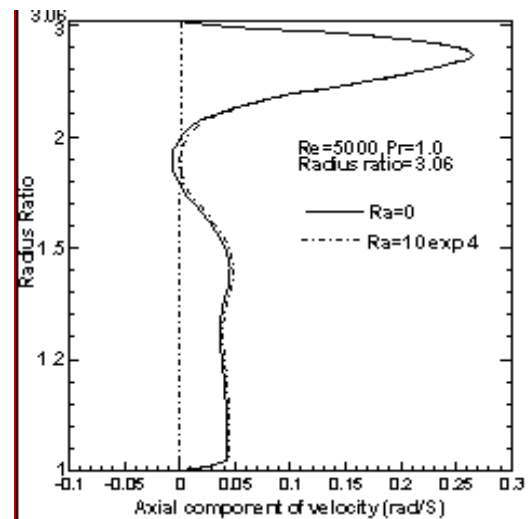
Fig. 9. Axial velocity variation along the truncated conical axis at θ_0=0, for Re =5000 α=3.06.

centrifugally unbalanced redistribution of the angular momentum in the central swirl core flow (Lopez, 1990). The aim is to study the effect of Reynolds number and radius ratio on the formation, development, and breakdown of vortex bubbles in this type of type of geometric configuration.

Reynolds Number Effects

Figure 10 shows a series of streamlined plots at various critical Reynolds numbers. It represents a typical sequence for the appearance and the disappearance of the recirculation bubble for a fixed aspect ratio α=1.68. Figure 10a shows that the stagnation points and recirculation zones are not observed below rotational *Re* = 418. Below this rotation rate, the flow has a simple cellular structure similar to the previous case (low *Re* for α=1.68). The size of the central viscous core increases with increasing angular velocity imparted to it. With further increase in the swirl, a single breakdown bubble appears (Fig. 10b) at *Re* = 456. Two upstream and downstream stagnation points appear when the rotation rate increases to Re = 644. There are two well-defined vortex breakdown bubbles with distinct recirculation zones (Fig. 10c). The size of the recirculation zone upstream and downstream breakdown bubbles are diminished and separated with an increase in rotation
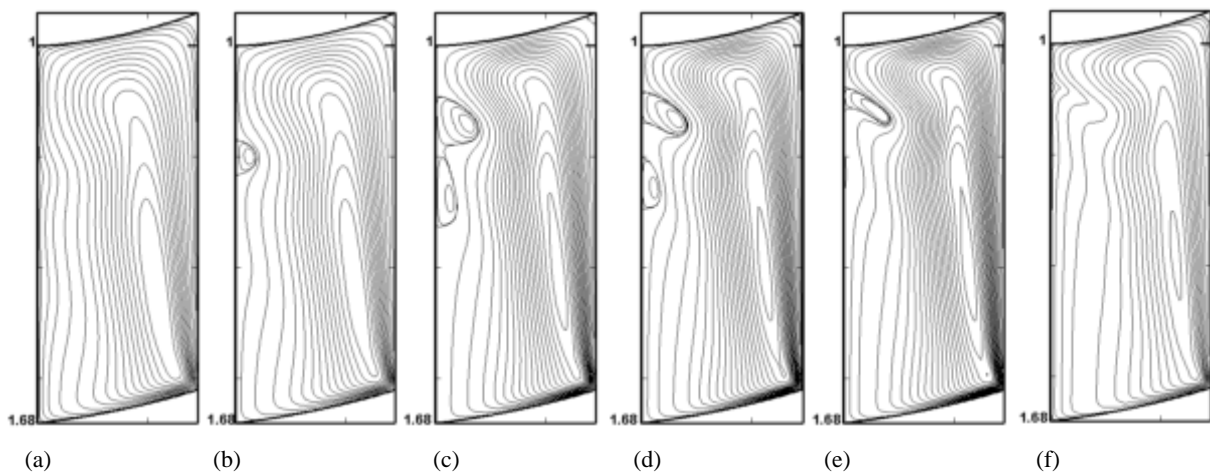
Fig. 10 A "typical" set of streamline plots showing the appearance and disappearance of the recirculation for $\alpha=1.68$, $\theta_0=20°$ and for different Re: (a) Re = 418, (b) Re =456, (c) Re =644, (d) Re =697, (e) Re =767, (f) Re =885

rate (Fig. 11d). They collapse to a single vortex breakdown as the Reynolds number increases to Re = 767 (Fig. 10e). When rotational rate reaches Re=885, vortex breakdown bubbles disappear. Steady results reveal that the occurrence of breakdown bubbles indicates the existence of a regime diagram analogous to those reported by Escudier (1984). The flow becomes unstable when the Reynolds number exceeds the critical Reynolds number Re_{c2}>767.

Figure 10 shows that when moving from top to the bottom wall for a given Reynolds number, the axial component of velocity alongside the axis in the beginning rises to its highest value at a short range from the fixed upper disk. After, it begins to decrease and then exhibits the oscillating configuration. Furthermore, the speed component disappears at each stagnation point before changing the signs. It indicates a change in an axial flow direction that highlights the occurrence of vortex failure. These zones appear spontaneously, following to a break of the balance between the centrifugal force and the radial pressure gradient characterizing the cylindrical core in quasi-solid rotation. The occurrence of recirculation zones is promoted by the formation of an adverse pressure gradient on the axis of the cavity causing the slowing down of the axial velocity until the formation of a stagnation point, followed by a deviation (divergence) of current lines. Within the bubbles thus evolved, the flow changes direction.

Radius Ratio Effects

The vortex region results are examined to highlight the changes that occur with increasing radius ratio in the range $1.48<\alpha<3.06$ and for a fixed value of Reynolds number Re=644. These particular parameters were chosen for both reasons; first to highlight and analyze the phenomenon of vortex breakdown in new geometries, second can present show one, two well-configured axisymmetric reverse zones. The aim is to explore a wider range of parameters. The steam contours (Fig.12) exhibit the flow comportment in the plan (r,θ) are coherent with the regions and boundary diagram made by Escudier (1984). For $\alpha=1.48$ case, streamlines nearby of
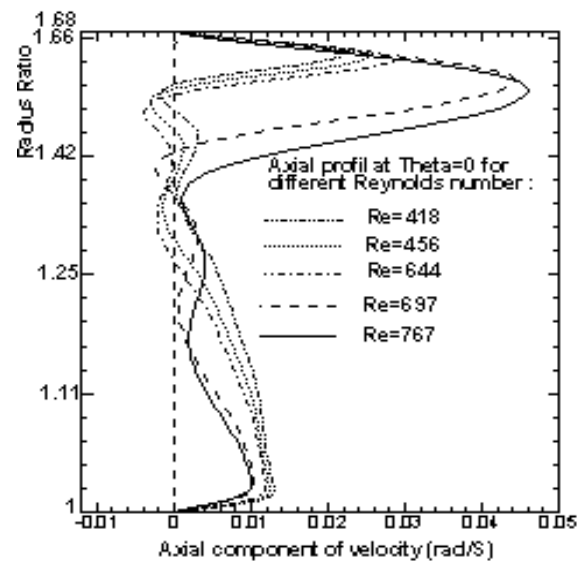
Fig. 11 Axial velocity on the axis of cylinder for $\alpha=1.68$, $\theta_0=20°$ and for different Reynolds number: Re=418,456,644,697,767

the center of symmetry are aligned, indicating no sign of vortex breakdown (Fig. 12a). For the case $\alpha=1.58$, only one vortex structure appears (Fig. 12b), while for a value of radius ratio equal to $\alpha=1.78$, two breakdowns well developed occur in succession along the axis rotation (Fig. 12d). At the highest value of α $(\alpha>1.78)$, the suppression of the bubble can be observed. Figure 13 clearly confirms the disappearance of the two bulbs beyond radius ratio equal to 2.

3.2.2 Differential Rotation Effect of the Spherical Endwalls

The fundamental flow comportment, motivated per the two end disks of a cylindrical enclosure, is showed in Fig. 13, for the following specific parameters Re= 440, $0.07 \leq S \leq -0.045$, $\alpha=1.58$. This case was selected because exceptional results are observed and the rotation of the bottom of the cavity acquires the fluid an azimuth movement, consequently, a development of the secondary circulation which breaks to give a well developed zone called burst (Fig. 14a).

(a)α=1.48   (b) α=1.58   (c)α=1.78   (d)α=3.06
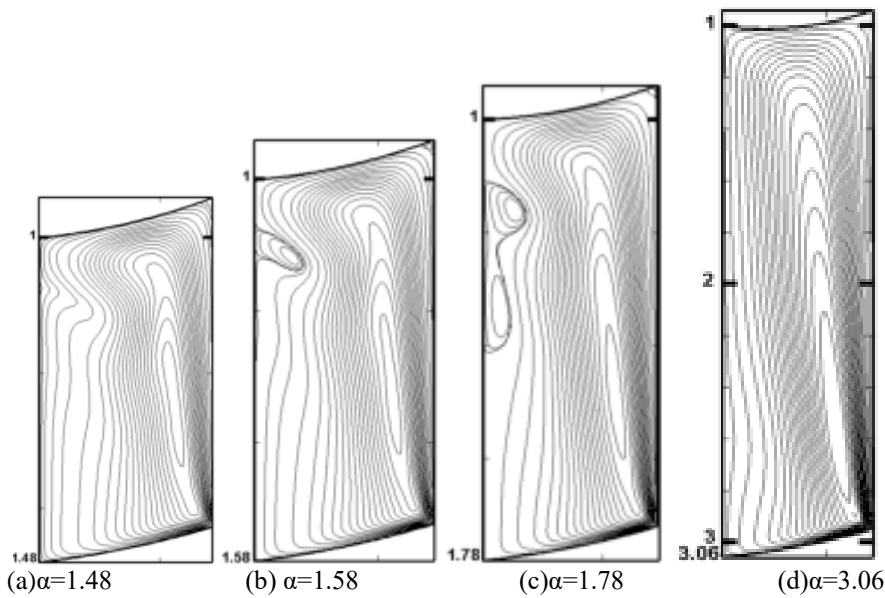
Fig. 12 Meridian streamlines showing the effect of radius ratio for Re=644, θ_0=20. The radius ratio α is indicated
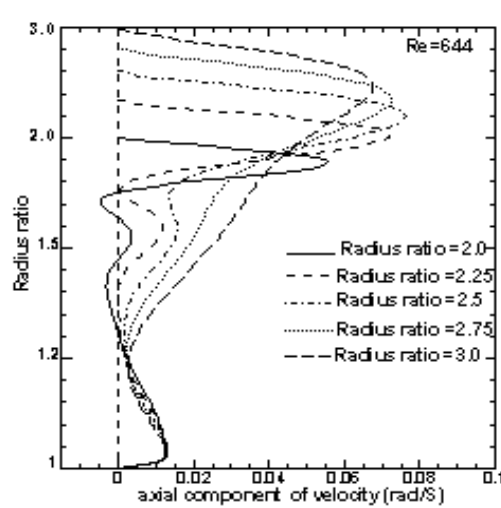
Fig. 13 Axial velocity on the axis for different cylinders for Re=644, θ_0=20

(a)   (b)   (c)
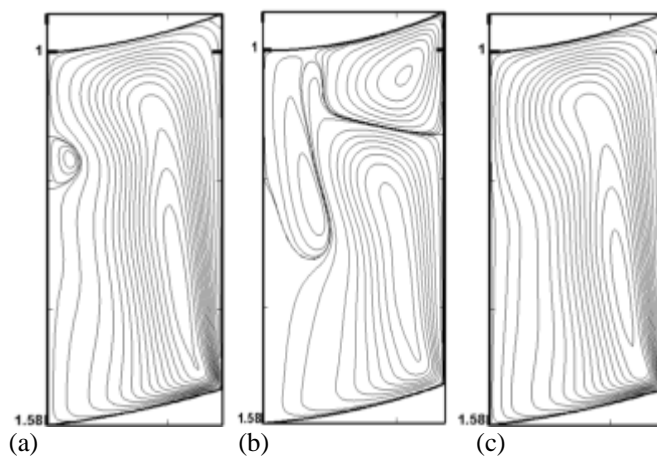
Fig. 14 Contours of stream function showing the effect of differential rotations of the spherical end walls : (a) without rotation, (b) with co-rotation, (c) with counter-rotation for Re=440, α=1.58, θ_0=20°

Qualitatively, the results indicate that for a weak co-rotation of the top spherical disk (0.070=S=0.2), the dimension of the bubble swells significantly with the growing velocity ratio with appearance a wedge vortex in the upper right-side corner of the meridian plan. The competition of the outward circulations induced by end disks produces a great pertinent change to the vortex breakdown by coalesces of the two regions zones. It provokes a stagnation point on the cylindrical wall and a decollement point on the axis of rotation of the cavity
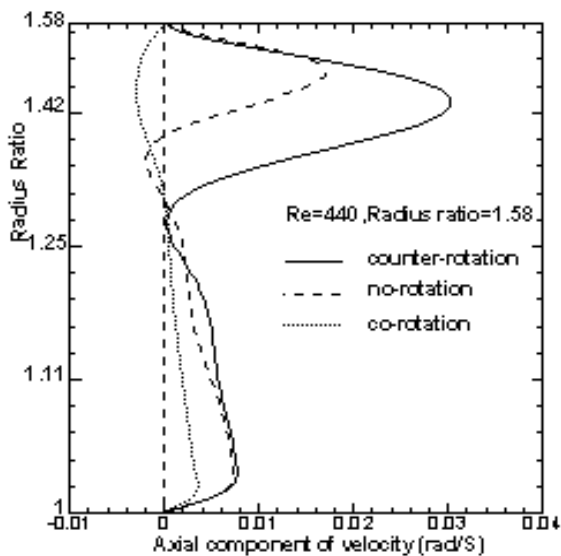
Fig. 15 Axial velocity along axis for Re=440, α=1.58, θ₀=20°

(Fig. 14b). By contrast, the flow induced per the counter-rotating of both endwalls of the cylindrical cavity tends to diminish the bubble slowly when the velocity ratio is increased. It completely vanishes (Fig. 14c).

Figure 15 shows the difference between co- and counter-rotation, where axial velocities along the cylinder axis are plotted. The recirculation region extending up to 72% of the cylinder height develops for the co-rotation of the upper and lower disc. In contrast, there is no backflow for counter-rotation. The stagnation point separating the dominant zone results from the competition of centrifugal contra-rotating circulations coupled with each rotation disc. Indeed, the flow centrifuged by the fastest disc is channelled axially by the fixed side wall to the slower disc. At the same time, the flow adhering to the latter undergoes centrifugal counter-rotating circulation at a rotation rate ratio. Also, Fig. 15 illustrates the upper wall without rotation with a vortex breakdown bubble. It shows the contrast between these two diverse cases.
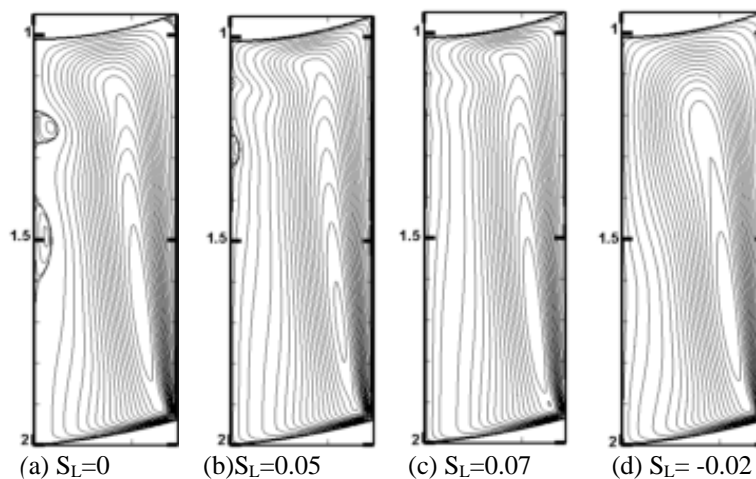
3.2.3 Differential Rotation Effects of the Sidewall

Regarding the kinematical control of the breakdown, it can be noted that a differential rotation of the sidewall with the physical parameter $S_L=\Omega_L / \Omega_b$ could cause a modification of the vortex structure, depending on the rate and direction of rotation. In this study, a new model of a rotating flow in an enclosure of radius ratio α=2 is controlled, whereas Re=590. This behaviour is favoured because of the appearance of two separate bubbles on polar axis and hence a more challenging one. To investigate the impact of varying the kinematic provisos upstream, the vortex bubbles (Fig. 16b) get stretched in the axial direction and slightly shifts upward for weak sidewall co-rotations sufficient to suppress, successively, the two bubbles beyond $S_L=0.07$ (Fig. 16c). We note that a strong co-rotation, promotes balance in the central body of the flow. The representations of Fig. 17 show that by increasing the rate of co-rotation of the side wall, the core expands and the whole fluid takes on a quasi-solid rotation.

In the case of a counter-rotation of the wall cylindrical, as shown by the iso-lines of the current function in the Fig. 16d, there is an intensification of the descending axial flow of the Bôdewadt shear layer formed on the fixed spherical disc, which pushes the stagnation points downwards by successively suppressing the two bubbles.

3.3 Investigation in the Hemispherical

The basic flow comportment is performed systematically for a region between two hemispheres concentric with a free surface condition when the internal hemisphere revolves with a specific value of rotational speed Ω_t. In contrast, the outside hemisphere is immobile in the second case, when the outer hemispherical shell revolves with a specific value of rotational speed Ω_b, whereas the inner hemisphere is at standstill. The numerical simulation shows various secondary flow structures due to the combined effects of the rotating and/or stationary boundaries, whose nature depends on the physical parameters Re=$\Omega_b R_{0b}^2/\nu$ (the Reynolds number).

(a) $S_L=0$ (b)$S_L=0.05$ (c) $S_L=0.07$ (d) $S_L= -0.02$

Fig. 16 Effect of differential rotation of the sidewall. Streamlines pattern for Re=590, α=2, θ₀=20°. The rotation ratio S_L is indicated

(a)S_L=0   (b)S_L=0.08   (c)S_L=0.3   (d)S_L=0.5
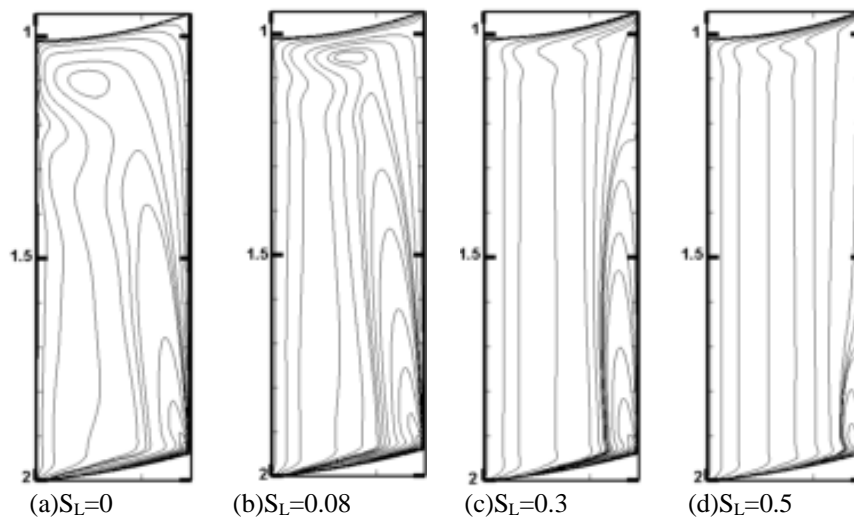
Fig. 17 Effect of differential rotation of the sidewall. Contours of angular momentum pattern for Re=590, α=2, θ_0=20°. The rotation ratio S_L is indicated

(a)Re=766   (b) Re=100
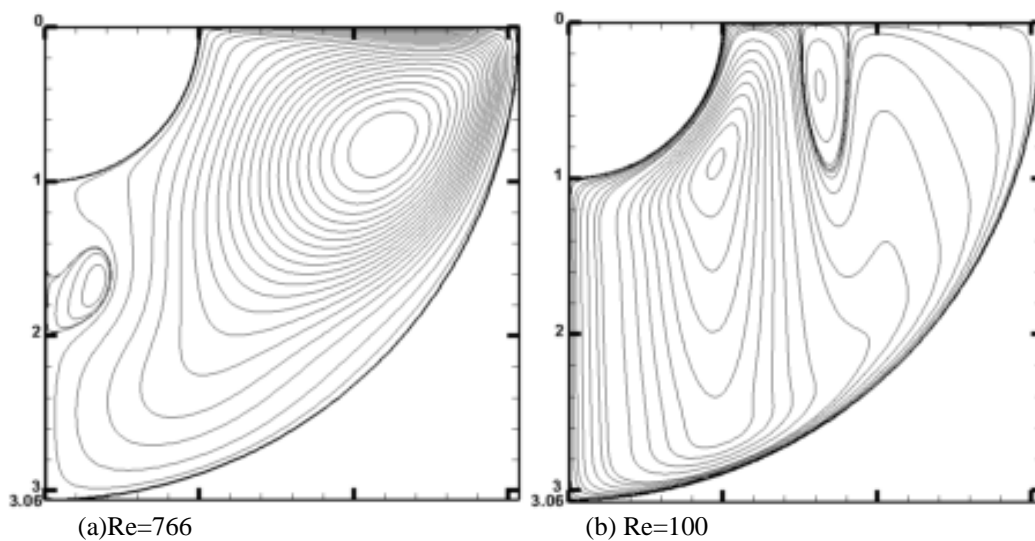
Fig. 18 Contours of Ψ for α= 3.06, θ_0= 90°

For a couple of particular parameters (α= 3.06, Re= 766) corresponding to the first case, the stream comportment is sleek for (Re< Re_{cr}). When the value of the dynamic parameter greater than the critical Reynolds number, a closed recirculating region in their structure limited by two stagnation points on the rotating axis, as show in Fig. 18a. However, the configuration corresponds to the second case, a clockwise toric segregated type of overturned flow, attached to the open surface under a couple particular parameters a=3.06, Re=100, as evidenced quantitatively in Fig. 18b.

Calculations show that the kinematics conditions considerably affect the topology on the vortex flows. For a particular parameter pair 0.01≤S_o≤0.05, Re= 1222, α= 3.06, the impact of altering the kinematics provisos upstream of the vortex breakdown (Fig. 19b) denotes that a relatively feeble co-rotation of the inner hemisphere is sufficient to suppress the toroidal vortex on the equator while maintaining steady flow. We also note that the streamlines are practically vertical in the vicinity of the polar axis, indicating near-uniform axial velocity, after control.

Conversely, meridian streamlines show that a weak counter-rotation (S_o= -0.01) tends to suppress the toroidal structure, accompanied by forming a recirculation zone near the outer hemisphere's surface (Fig. 19c, Fig.19d). Moreover, this separated region extends considerably with the stagnation and reattachment points approaching respectively the axis of rotation and the surface of the plane of the equator as the rate |S| grows.

4. CONCLUSION

This study investigated axisymmetric vortex flows generated by rotating spherical end discs of different cavities. The structure of multiple zones (axis bubbles and/or toroidal vortex decomposition) was investigated as a function of varying specific parameters (α, Re). Furthermore, we analysed how these zones are controlled in their development. The following conclusions are therefore drawn from this study:

The introduction of a conical lid high above h_c =0.04m in place of the spherical disc has a dominant influence on the removal of vortex failure. Therefore, a

(a) $S_o = 0$ (b) $S_o = 0.05$

(c) $S_o = -0.008$ (d) $S_o = -0.01$
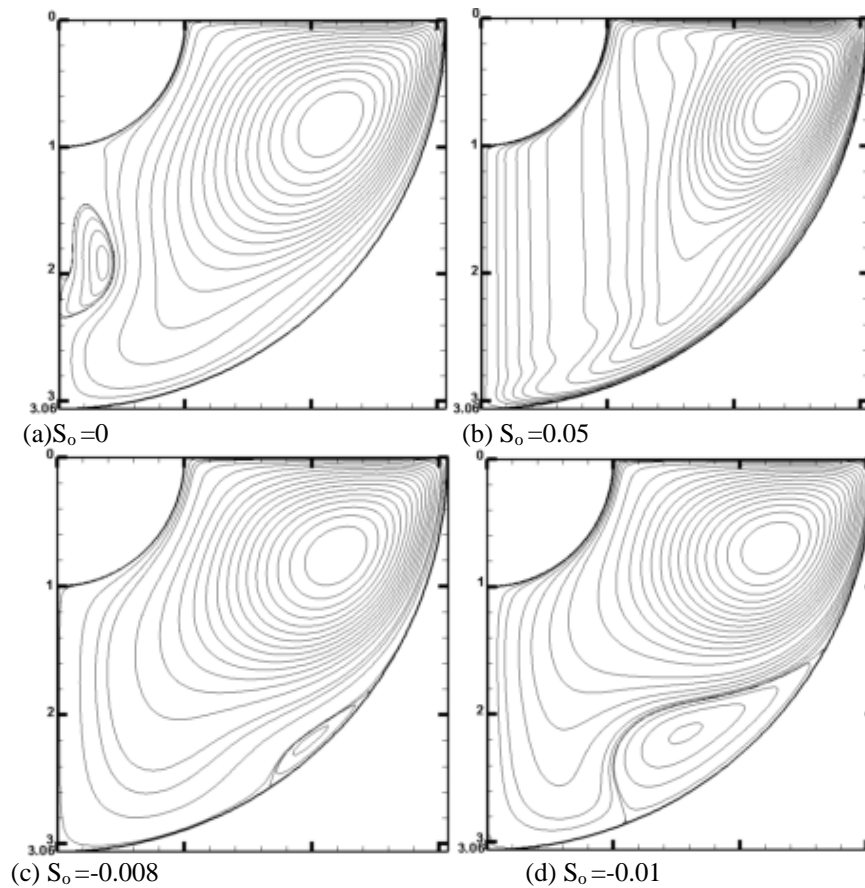
Fig. 19 Contours of Ψ for Re=1222, α=3.06, θ_0=90°, S_0 is indicated

flow pattern that is dominated by a co-rotation of an upper tapered cover intensifies the vortex and accelerates the creation of bubbles. While counter rotation functions in opposite ways, the formation of bubbles is delayed.

The solutions based on the influence of a slight inclination of the conical side wall revealed acceleration and an intensification of the axial flow emanating from the fixed disc, causing the progressive disappearance of the burst zones under the influence of a slight inclination gradual side wall.

Depending on the direction and the rate of differential rotation of the walls of the cylindrical cavity, we have shown that the induced meridian circulation can stimulate the formation of burst ones or contribute to eliminate them.

An axial temperature gradient, directed in the direction of the base flow (Ra > 0) reduces the Ekman pumping effect so that the meridian flow remains confined to the vicinity of the rotating disc, as a result eliminates the vortex structure; while that directed in the opposite direction to the basic flow (Ra < 0), stimulates their appearance. For these gradients, convective transport is dominant in the flow.

ACKNOWLEDGEMENTS

CONFLICT OF INTEREST

The authors declare that there is no known conflict of interest associated with this publication

AUTHORS CONTRIBUTION

The authors made a substantial contribution to the design of the article. The numerical simulation was performed by Ms A. Meziane and Dr M. Imoula. Pr M. Hachemi contributed to the analysis and interpretation of the data; Dr M. Imoula and Mrs A.Meziane wrote the article . Pr M. Kessal and Pr M. Hachemi critically reviewed the content and approved the vesion to be published.

REFERENCES

Bhaumik, S. K., & Lakshmisha, K. N. (2007). Lattice boltzmann simulation of the lid-diven swirling flow in a confined cylindrical cavity. *Computers fluids*, 36(7), 1163-173. https://doi.org/10.1016/j.compfluid.2007.02.001

Bühler, K. (2009). Pattern formation in rotating fluids. *Journal of Thermal Science*, 18(2), 109-118. https://doi.org/10.1007/s11630-009-0109-2

Cabeza, C., Sarasúa, G., Marti, A. C., & Bove, I. (2005). A simple mechanism for controlling vortex breakdown in a closed flow. *Arxiv Preprint Physics, 0512248*.

https://doi.org/10.48550/arXiv.physics/0512248

Dash, S., & Singh, N. (2016). Effects of partial heating of top rotating lid with axial temperature gradient on vortex breakdown in case of axisymmetric stratified lid-driven swirling flow. *Yildiz Technical University Press, Istanbul, Turkey J. Thermal Eng*, 2, 883-896. https://eds.yildiz.edu.tr/journal-of-thermal-engineering/Articles

Dash, S. C., & Singh, N. (2018). Stability boundaries for vortex breakdowns and boundaries between oscillatory and steady swirling flow in a cylindrical annulus with a top rotating lid. *Journal of the Brazilian Society of Mechanical Sciences and Engineering*, 40(7), 1-19. https://doi.org/10.1007/s40430-018-1256-8

Escudier, M. P. (1984). Observations of the flow produced in a cylindrical container by a rotating endwall. *Experiments in fluids*, 2(4), 189-196. https://doi.org/10.1007/BF00571864

Escudier, M. P., J. O'Leary, & Poole, R. J. (2007). Flow produced in a conical Container by a rotating endwall. *International Journal of Heat and Fluid Flow*, 28(6), 1418-1428. https://doi.org/10.1016/j.ijheatfluidflow.2007.04.018

Herrada, M. A., & Shtern, V. (2003). Vortex breakdown control by adding near-axis swirl and temperature gradients. *Physical Review E*, 68(4), 041202. https://doi.org/10.1103/PhysRevE.68.041202

Husain, H. S., Shtern, V., & Hussain, F. (2003). Control of vortex breakdown by addition of near-axis swirl. *Physics of Fluids*, 15(2), 271-279. https://doi.org/10.1063/1.1530161

Imoula, M., Saci, R., Benkoussas, B., & Gatignol, R. (2016). Characterization of swirling flows in a partly open cylinder. *Journal of Applied Fluid Mechanics*, 9(6), 3167-3176. https://doi.org/10.29252/JAFM.09.06.26281.

Jacono, D. L., Sørensen, J. N., Thompson, M. C., & Hourigan, K. (2008). Control of vortex breakdown in a closed cylinder with a small rotating rod. *Journal of Fluids and Structures*, 24(8), 1278-1283. https://doi.org/10.1016/j.jfluidstructs.2008.06.015

Leibovich, S. (1978). The structure of vortex breakdown. *Annual Review of Fluid Mechanics*, 10(1), 221-246. https://doi.org/10.1146/annurev.fl.10.010178.001253

Lopez, J. M. (1990). Axisymmetric vortex breakdown flow. *Journal of Fluid Mechanics*, 221, 533-552. https://doi.org/10.1017/S0022112090003664

Meunier, P., & Hourigan, K. (2013). Mixing in a vortex breakdown flow. *Journal of Fluid Mechanics*, 731, 195. https://doi.org/10.1017/jfm.2013.226

Mununga, L., Jacono, D. L., Sorensen, J. N., Leweke, T., Thompson, M. C., & Hourigan, K. (2014). Control of confined vortex breakdown with partial rotating lids. *Journal of Fluid Mechanics*, 738, 5-33. https://doi.org/10.1017/jfm.2013.596

Pereira, J. C. F., & Sousa, J. M. M. (1997). Steady and transient topologies of confined vortex breakdown generated by a rotating cone. *Opti. Diag. Eng*, 2, 61-70. http://www.lasef.ist.utl.pt/lasef/

Rudolf, P. A. V. E. L. (2008). *Simulation of vortex breakdown in an enclosed cylinder as a preliminary study of the draft tube vortex rope creation.* Proceedings of the WSEAS Fluid Mechanics Conference, Rhodos. http://khzs.fme.vutbr.cz/~rudolf

Serre, E., & Bontoux, P. (2001). Eclatement tourbillonnaire dans une cavité rotor–stator cylindrique. *Comptes Rendus de l'Académie des Sciences-Series IIB- Mechanics*, 329(9), 671-677. https://doi.org/10.1016/S1620-7742(01)01385-X

Sousa, J. M. M. (2008). Steady vortex breakdown in swirling flow inside a closed container: Numerical simulations, PIV and LDV measurements. *The Open Mechanical Engineering Journal*, 2(1). https://doi.org/10.2174/1874155X00802010069

Sturzenegger, J. C., Sarasúa, L. G., & Martí, A. C. (2012). Analytical solutions for the axisymmetric flow inside a cylindrical container with a rod along the axis at low Reynolds numbers. *Journal of Fluids and Structures*, 28, 473-479. https://doi.org/10.1016/j.jfluidstructs.2011.11.002

Turan, O., Yigit, S., & Chakraborty, N. (2018). Effects of wall heating on laminar mixed convection in a cylindrical enclosure with a rotating end wall. *International Journal of Thermal Sciences*, 131, 80-93. https://doi.org/10.1016/j.ijthermalsci.2018.05.005

Vogel, H. U. (1968). *Experimetelle ergebnisse ueber die laminare stroemung in einem zylindrischen gehaeuse mit darin rotierender scheibe*. Max-Planck-Instiut fur Stromung- sforschung, Gottingen Bericht, 6. https://cir.nii.ac.jp/crid/1571698599901859968

Yalagach, A., & Salih, A. (2016). Study of vortex breakdown in a cylindrical cavity with a rotating endwall. *International Journal of FluidMechanics Research*, 43(3). https://www.dl.begellhouse.com/journals/71cb29ca5b40f8f8,2404c1223f03c958,3ca81cf80d27c2c7.html

Yu, Y., Li, B. W., & Thess, A. (2013). The effect of a uniform magnetic field on vortex breakdown in a cylinder with a rotating upper lid. *Computers &Fluids*, 88, 510-523. https://doi.org/10.1016/j.compfluid.2013.10.006